21st Australasian Fluid Mechanics Conference
Adelaide, Australia
10-13 December 2018

Horizontal Convection: Shallow Enclosures Confine Heating and Cooling Near Sidewalls

Sajjad Hossain, Tony Vo and Gregory J. Sheard

Department of Mechanical and Aerospace Engineering
Monash University, Victoria 3800, Australia

Abstract

Horizontal convection is investigated numerically in shallow rectangular enclosures with height-to-length aspect ratios up to 160 times shallower than that has been studied previously to determine the effect of ocean-relevant aspect ratio confinement on horizontal convection. Simulations are conducted at a Prandtl number of Pr = 6.14 (consistent with water) across a wide span of Rayleigh numbers, ($10 \leq Ra \leq 10^{16}$) and aspect ratios ($10^{-3} \leq A \leq 0.16$). A critical Ra is found marking the transition between the diffusion-dominated and convective regimes across these small aspect ratios. The heat transfer scalings governing these regimes are determined as a function of aspect ratio. The critical Nu and Ra are found to closely fit power-law scalings $Ra \propto A^{-4}$ and $Nu \propto Ra^{-1/4}$. These scalings lead to modified Nu and Ra parameters found to control the flow at lower Rayleigh numbers, which provide evidence that at lower Ra, the height of the enclosure controls the flow dynamics. Furthermore, a previously unseen behaviour is discovered whereby decreasing aspect ratio of the enclosure, the formation of an increasingly large horizontally uniform zone is evident, which implies that the heating and cooling increasingly confined to regions close to the end-walls.

Introduction

Horizontal convection is a distinctive class of natural convection, where non-uniform heating and cooling occurs along just one horizontal boundary of the enclosure. In contrast to the substantially studied Rayleigh–Bénard convection, where convective overturning circulation is stimulated by both heating and cooling, the strength of overturning circulation in horizontal convection is ultimately limited by heat diffusion [1]. Studies of horizontal convection have been inspired by the transport of warm fluids in the oceanic circulation and engineering processes, like glass melting in furnaces [2]. Several experimental and numerical studies on horizontal convection investigated the flow dynamics and heat transfer scalings. Experiments by Mullarney et al. [3] with water in an enclosure of aspect ratio (height to length), A=0.16 showed that beyond the diffusion-dominated regime, the Nusselt number (Nu) scales approximately with $Ra^{1/5}$, which is similar to the Rossby scaling [4]. Chiu-Webster et al. [5] studied horizontal convection in the infinite-Prandtl number limit relevant to very viscous fluids at a range of A and Ra with highest values of 2 and 10^{10}, respectively. The authors also recovered the Rossby scaling of $Nu \propto Ra^{1/5}$ and provided evidence of aspect ratio independence of this scaling for $Ra > 10^7$. However, Siggers et al. [6] used a variational analysis to report a higher upper bound of the scaling, namely $Nu \propto Ra^{1/3}$. Sheard and King [7] used a spectral element method to investigate horizontal convection for aspect ratios, $0.16 \leq A \leq 2.0$ at a range of Rayleigh and fixed Prandtl number representative of water (Pr = 6.14). They reported an aspect ratio dependence based on the measured Nu and boundary layer thickness at low Ra. The authors also confirmed an increase in the exponent of Ra 1/5th to 1/3rd in the convective regime for the Nu scaling. This uplift was later shown to represent a shift between flow regimes both obeying $Nu \propto Ra^{1/5}$ [8].

Despite the substantial motivation to study horizontal convection to reveal the role of buoyancy forcing in ocean currents, the previously investigated range of enclosure aspect ratios ($A \geq 0.16$) is at least two orders of magnitude larger compared to the ocean-relevant values ($10^{-5} \leq O(A) \leq 10^{-3}$). Therefore, the impact of small aspect ratios (i.e. the confinement of the enclosures) on the governing parameters of horizontal convection remains unexplored. This study emphasises on providing insights into enclosure confinement of horizontal convection.

Methodology

The computation domain consists of a rectangular enclosure, having internal dimensions of length L, height, H (aspect ratio, A= H/L) as shown in figure 1. The flow is driven by a linear temperature profile applied along the bottom boundary of the enclosure. The side and top walls are thermally insulated (a zero wall-normal temperature gradient is imposed), and a no-slip condition is imposed on the velocity field on all walls. The buoyancy is modelled with the Boussinesq approximation, in

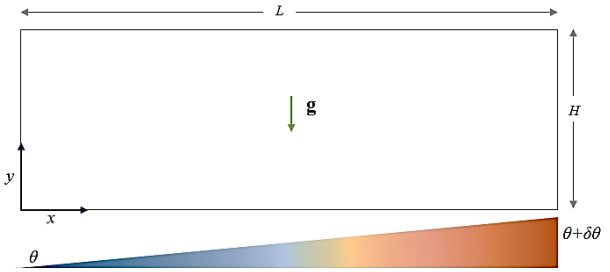

Figure 1. A schematic diagram of the system. The origin of the coordinate system placed at the bottom-left corner, and a temperature difference of δθ imposed along the bottom boundary.

which density differences in the fluid are disregarded except for the contribution of gravity. The Navier–Stokes equations governing a Boussinesq fluid are written as

$$\frac{\partial \mathbf{u}}{\partial t} = -(\mathbf{u}\cdot\boldsymbol{\nabla})\mathbf{u} - \boldsymbol{\nabla} p + Pr\nabla^2\mathbf{u} - PrRa\hat{\mathbf{g}}\theta, \quad (1)$$

$$\boldsymbol{\nabla}\cdot\mathbf{u} = 0, \quad (2)$$

$$\frac{\partial \theta}{\partial t} = -(\mathbf{u}\cdot\boldsymbol{\nabla})\theta + \nabla^2\theta, \quad (3)$$

where t is time, θ is the temperature, p is the pressure, $\boldsymbol{u}$ denotes the velocity vector and $\hat{\mathbf{g}}$ is a unit vector in the direction of gravity. In the governing equations, lengths, time, velocity, pressure and temperature difference are respectively scaled by L, L^2/κ, κ/L, $\rho_\circ \kappa^2/L^2$ and δθ. Here, $\rho_\circ$ and κ are defined as the reference density of the fluid and thermal diffusivity. The 2D incompressible Navier–Stokes equations augmented by a buoyancy term in the momentum equation and a scalar advection-diffusion transport equation for temperature are solved by a high-order in-house solver, which employs a spectral-element method for spatial discretisation and a 3rd-order time integration scheme based on backwards-

differencing. Meshes are constructed for various aspect ratios from $A = 0.16$ down to 0.001. The number of spectral elements in the meshes varies between 296 and 4128. The elements are concentrated near the sidewalls; and adjacent to the hot bottom end boundary to ensure that flow is resolved, while relaxing the mesh density in the interior. The highest aspect ratio considered in this study (0.16) corresponds to the lowest aspect ratio previously considered in the literature. After a thorough grid resolution study, a polynomial order of 5 was selected to conduct the study considering a trade-off between computational cost and accuracy.

Results

The Nusselt number is calculated from the obtained flux values along the bottom horizontal boundary of the enclosure for each aspect ratio configuration, and these are plotted against the Rayleigh number in figure 2. Nusselt number is found to be directly proportional to the aspect ratios ($Nu \sim A$) and independent of Rayleigh number at low Rayleigh numbers: this range of Rayleigh numbers is identified as the diffusion-dominated or conduction regime. With an increase in Rayleigh number, the Nusselt number for all aspect ratios demonstrate a rapid rise in the transition regime before collapsing onto a single line: this region is identified as the convective regime. The results show that by increasing enclosure confinement, i.e. towards smaller aspect ratios, the onset of the transition regimes delays to a higher Rayleigh number. The onset of the transition regime is quantified by introducing a critical value of Rayleigh and Nusselt number for each aspect ratio. A 5% deviation from the Rayleigh-number-independent value of the Nusselt number is taken to mark the critical Rayleigh number. The critical Nusselt and Rayleigh numbers are found to closely fit power-law scalings having $Ra \propto A^{-4}$ and $Nu \propto Ra^{-1/4}$.

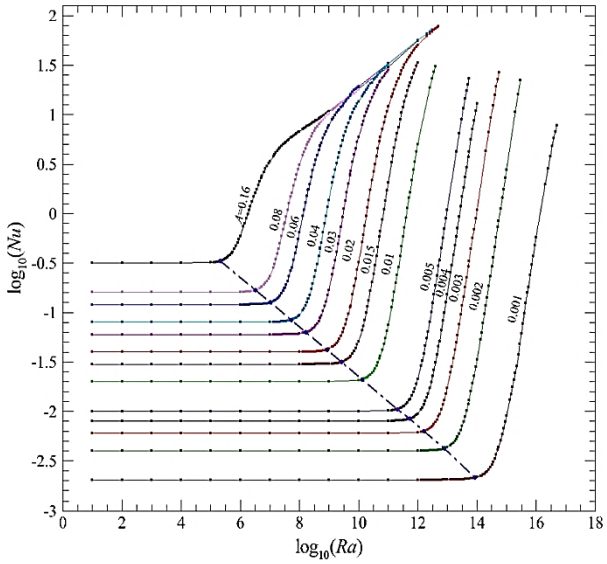

Figure 2. A plot of $\log_{10}(Nu)$ against $\log_{10}(Ra)$ for $10^{-3} \leq A \leq 0.16$. The dotted line marks the onset of the transition regime.

Based on the low-Ra/low-A scalings of $Ra \sim A^{-4}$ and $Nu \sim A$, figure 2 can be rescaled and plotted as Nu / A against $Ra.A^4$, the outcome of which is shown in figure 3. It shows that beyond the critical Ra_H, Nu / A values for all aspect ratio start branching off from the highest A=0.16 to the lowest A=0.001 with increasing Rayleigh number, which resembles the opposite of the collapse in Nu-Ra plot in the convection dominated regime. For lower values of RaA^4, the corresponding values of Nu / A have collapsed into a single line, which is consistent for all of

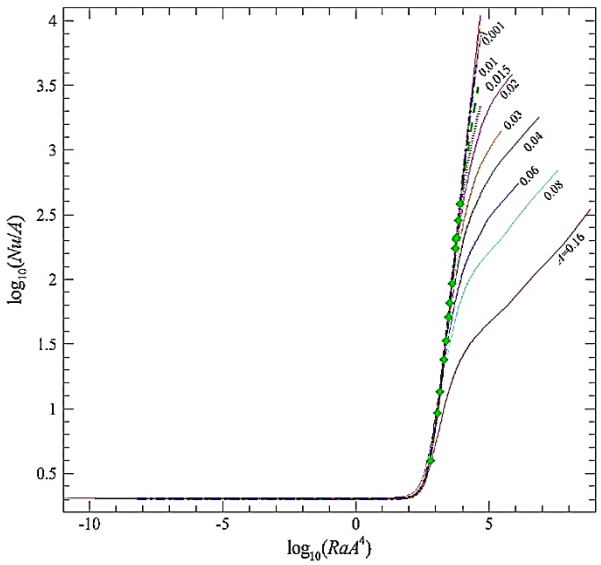

Figure 3. The Nu-Ra plot is rescaled with $Ra \sim A^{-4}$ and $Nu \sim A$ to investigate the self-similarity features in the low Rayleigh number region.

the aspect ratios. This collapse indicates that the flow in this region is only governed by the height of the enclosure, which may be understood through modified Nusselt and Rayleigh numbers defined as

$$Ra^* = RaA^4 = \frac{g\alpha(\delta\theta_H)}{\upsilon\kappa_T} H^3, \tag{4}$$

$$Nu^* = \frac{Nu}{A} = \frac{F_T L}{\rho_\circ C_p \kappa_T (\delta\theta_H)}, \tag{5}$$

Here, $\delta\theta_H$ is the temperature difference along a portion of the bottom boundary of length H; this appears in both definitions. Additionally, note that L has been replaced by H as the characteristic length quantity appearing in the modified Rayleigh number definition. The corollary to this is that in very shallow enclosures, horizontal convection will be insensitive to the overall length of the enclosure; rather its behaviour will be controlled by the enclosure height and the horizontal temperature gradient acting over that same scale.

This collapsed region is further investigated by exploring the velocity and temperature contours of the aspect ratio range. For a modified rayleigh number, $Ra^* = 1.75$, the profile of the horizontal component of velocity is extracted at various horizontal locations within the shallow enclosures. The extraction points are selected based on different distances from the hot end, and expressed as a function of the enclosure height to explore corollary regarding the modified Rayleigh and Nusselt numbers in equation (4) and (5). The extracted velocities were normalized by the maximum value from each profile, while the vertical coordinate was normalised by enclosure height. Results are shown in figure 4, which presents the combined velocity profiles for all aspect ratios at a single value of $Ra.A^4$ within the collapsed regime.

The normalized profiles exhibit a strong collapse to a universal profile, implying a self-similarity in the velocity fields in this regime. By observing the extracted velocity data points for all aspect ratios throughout different locations (which are expressed in terms of the distance from the hot-end wall) along the horizontal boundary, it is evident from figure 5 that beyond a distance of approximately $4H$ (the distance from side-wall at

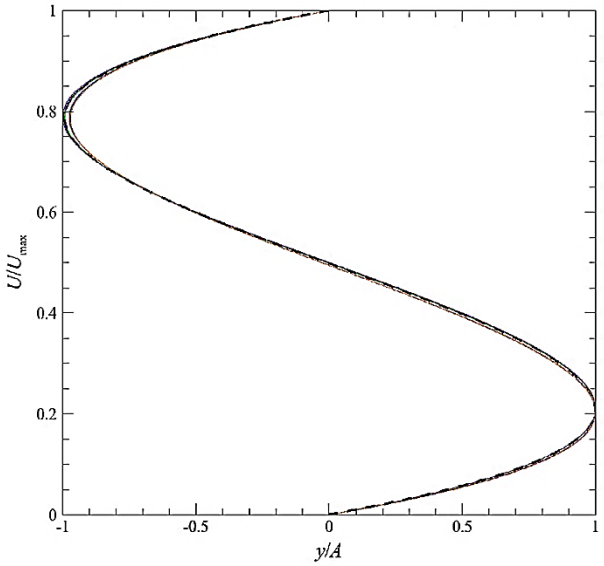

Figure 4. The velocity profiles generated from different locations throughout the horizontal bottom boundary are plotted with the analytical solution for modified Rayleigh number, Ra^*=1.75 and $10^{-3} \leq A \leq 0.16$.

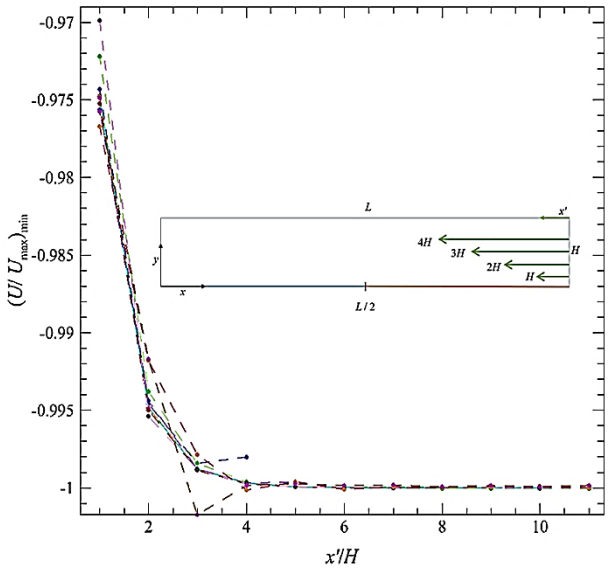

Figure 5. Minimum values of the scaled velocity plotted with the distance form hot-end wall. The distance is expressed in terms of the height of the enclosure. The inset figure demonstrates how the distance from the hot-end is calculated as a function of enclosure height.

the hot end of the enclosure-wall expressed as four times the height of enclosure), all data points consistently demonstrate a collapse to a single value. This trend demonstrates that the effects of the sidewalls in conduction-dominated horizontal convection are confined to within 4H from the wall, and this distance scales with height, not the horizontal enclosure length. Away from these end-wall regions, the velocity profile is uniform across the horizontal extent of the enclosure. This behaviour will emerge in enclosures having $L > 8H$, or $H / L < 1/8$ ($A < 0.125$), which is shallower than the shallowest (A = 0.16) enclosure investigated previously.

Similarly, temperature profiles relative to the local bottom wall temperature are extracted and normalised by the vertical temperature difference of each profile. The results are shown in figure 6. In contrast to the velocity contour scaling, the temperature contours for all aspect ratios are not well-collapsed as the obtained values in the vicinity of the hot-end wall seem to deviate from the rest of the data sets. However, similar to the velocity contours, the temperature contours also demonstrate the self-similarity feature beyond the 4H distance from the end walls for all aspect ratios. Polynomial fits to the scaled velocity and temperature profiles are similar to the analytical solution for flow in a horizontal channel driven by a horizontal temperature gradient under a zero net horizontal flow constraint, which is given as

$$U = \frac{RaA^3}{12}(2y^3 - 3y^2 + y), \tag{6}$$

$$\theta' = \frac{RaA^5}{24}\left(\frac{y^5}{5} - \frac{y^4}{2} + \frac{y^3}{3}\right). \tag{7}$$

Equations (6) and (7) length, velocity and temperature is scaled by H / A, κA / H and $\delta\theta$, and hence are non- dimensionalised.

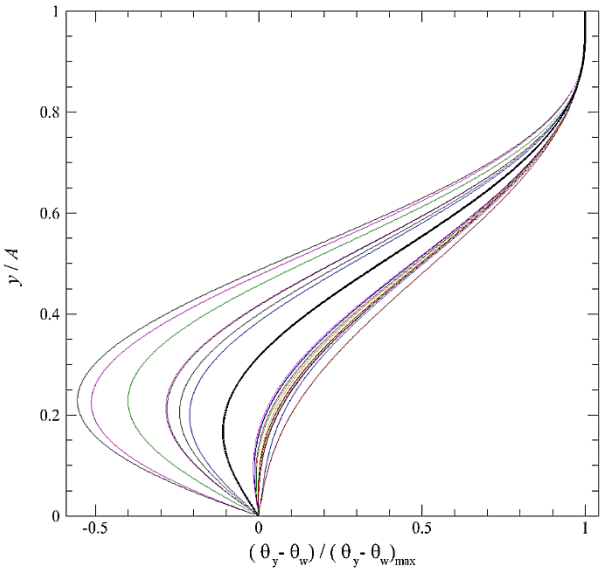

Figure 6. The temperature profiles generated from different locations throughout the horizontal bottom boundary plotted with the analytical solution for modified Rayleigh number, Ra^* = 1.75 and $10^{-3} \leq A \leq 0.16$. Here, θ_w is defined as the local bottom wall temperatures, and θ_y refers to fluid temperature along vertical axis.

Further analysis in the fluctuating temperature fields along the vertical axis of the enclosures of all aspect ratios provided new features. As the aspect ratio decreases, a region of horizontally independent temperature contours develops in the interior of the shallow enclosure. This region becomes more prominent as the aspect ratio gets smaller, until at the smallest (A=0.001) values almost all of the horizontal extent has horizontal isotherms, with changes confined to the near-wall regions. Figure 7 presents the obtained temperature fields for three chosen A-values from the range $10^{-3} \leq A \leq 0.16$ used in this study.

This horizontally independent region away from the end walls corresponds to the portion of the shallow enclosure that agrees with the analytical channel flow solution presented as equation (7), which has zero heat flux at the bottom boundary - hence heating and cooling are confined to the end-wall regions where the temperature fluctuation contours are not horizontally independent. It has been found that the turnover of the flow at each end of the enclosure is confined to 4H distance of the end-walls. Previously studied horizontal convection enclosure aspect ratios have been too large to detect this significant feature.

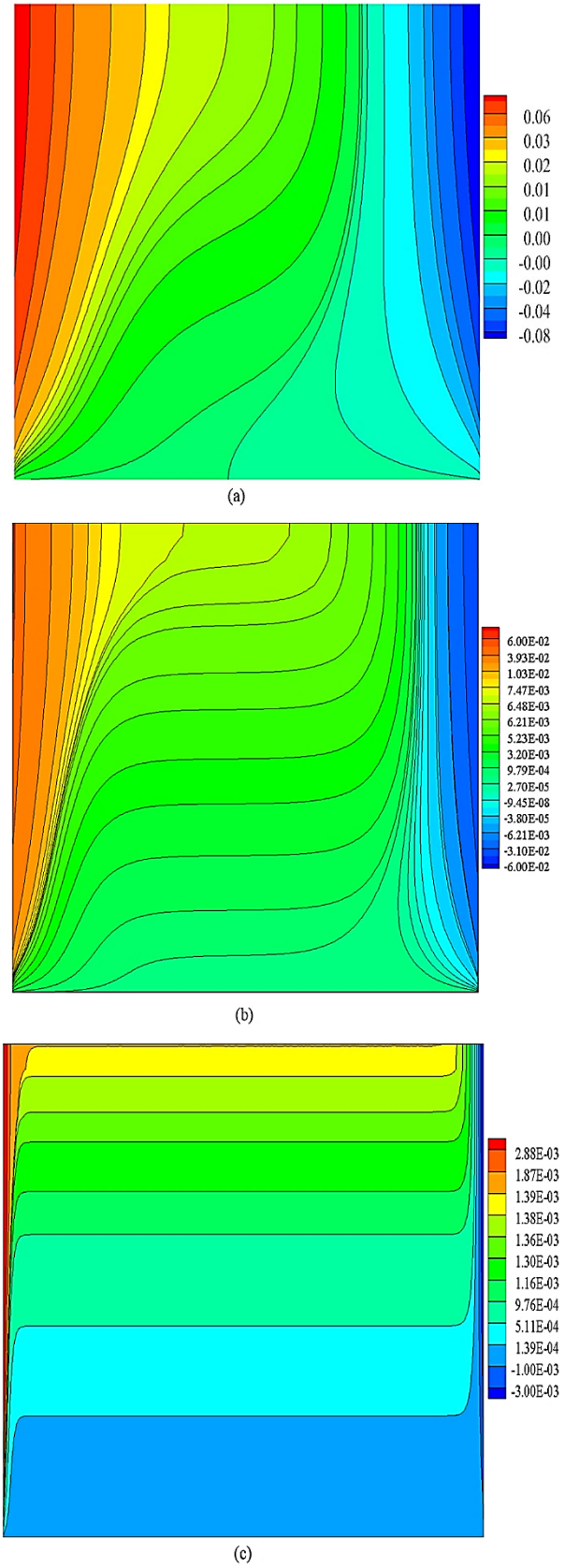

Figure 7. The contours of the temperature fluctuation of (a) A=0.16, (b) A=0.08 and (c) A=0.01. The vertical height of the contour plots has been increased to aid visualization. The contours are extracted for a modified Rayleigh number, $Ra^* = 1.75$.

Conclusions

Horizontal convection at ocean-relevant shallow enclosures with aspect ratios 160 times shallower than that of previous studies have been investigated emphasising the effect on enclosure confinement by employing high-resolution spectral element simulations. The heat transfer scalings with aspect ratio are proposed for different horizontal convection regimes. These scalings identified modified Rayleigh and Nusselt numbers that govern the low-Rayleigh-number conduction-dominated regime. These modified parameters reveal that low Rayleigh number shallow enclosures horizontal convection is controlled not by the enclosure width, but by its height. Furthermore, a previously unseen behaviour is discovered, whereby the turning of the flow at the enclosure sidewalls is confined to a small region near the walls, while away from the walls the flow is horizontally independent. The sidewall effects are confined to within a distance of approximately four times the enclosure height. This reveals that the shallowest enclosure previously investigated in the literature, the widely studied A = 0.16 enclosure, is not sufficiently shallow to capture these effects.

Acknowledgements

Sajjad Hossain is supported by Monash Graduate Scholarship (MGS) and Monash International Postgraduate Research Scholarship (MIPRS) from Monash University. This research was supported by the Australian Research Council through Discovery Grants DP150102920 and DP180102647 and was undertaken using the peak high performance computing facility of the National Computational Infrastructure (NCI) thanks to a grant under the National Computational Merit Allocation Scheme (NCMAS).

References

[1] Hughes, G.O. and R.W. Griffiths, Horizontal convection. Annu. Rev. Fluid Mech., 2008. 40: p. 185-208.

[2] Paparella, F., Turbulence, Horizontal Convection, and the Ocean's Meridional Overturning Circulation, in Mathematical Paradigms of Climate Science. 2016, Springer. p. 15-32.

[3] Mullarney, J.C., R.W. Griffiths, and G.O. Hughes, Convection driven by differential heating at a horizontal boundary. Journal of Fluid Mechanics, 2004. 516: p. 181-209.

[4] Rossby, H. On thermal convection driven by non-uniform heating from below: an experimental study. in Deep Sea Research and Oceanographic Abstracts. 1965. Elsevier.

[5] Chiu-Webster, S., E. Hinch, and J. Lister, Very viscous horizontal convection. Journal of Fluid Mechanics, 2008. 611: p. 395-426.

[6] Siggers, J., R. Kerswell, and N. Balmforth, Bounds on horizontal convection. Journal of Fluid Mechanics, 2004. 517: p. 55-70.

[7] Sheard, G.J. and M.P. King, Horizontal convection: effect of aspect ratio on Rayleigh number scaling and stability. Applied Mathematical Modelling, 2011. 35(4): p. 1647-1655.

[8] Gayen, B., R.W. Griffiths, and G.O. Hughes, Stability transitions and turbulence in horizontal convection. Journal of Fluid Mechanics, 2014. 751: p. 698-724.